

**Phonons in a one-dimensional Yukawa chain: Dusty plasma experiment and model**

Bin Liu\* and J. Goree†

*Department of Physics and Astronomy, The University of Iowa, Iowa City, Iowa 52242, USA*

(Received 11 November 2004; published 29 April 2005)

Phonons in a one-dimensional chain of charged microspheres suspended in a plasma were studied in an experiment. The phonons correspond to random particle motion in the chain; no external manipulation was applied to excite the phonons. Two modes were observed, longitudinal and transverse. The velocity fluctuations in the experiment are analyzed using current autocorrelation functions and a phonon spectrum. The phonon energy was found to be unequally partitioned among phonon modes in the dusty plasma experiment. The experimental phonon spectrum was characterized by a dispersion relation that was found to differ from the dispersion relation for externally excited phonons. This difference is attributed to the presence of frictional damping due to gas, which affects the propagation of externally excited phonons differently from phonons that correspond to random particle motion. A model is developed and fit to the experiment to explain the features of the autocorrelation function, phonon spectrum, and the dispersion relation.

DOI: 10.1103/PhysRevE.71.046410

PACS number(s): 52.27.Lw, 82.70.Dd, 52.27.Gr, 63.22.+m

**I. INTRODUCTION**

A one-dimensional (1D) chain is a simple form of condensed matter with low dimensionality. Recently, it has been studied in the fields of colloids, carbon nanotubes, and dusty plasmas. In colloidal suspensions, particles can be trapped in two counterpropagating laser beams to form a 1D coupled array that exhibits oscillations [1]. In a carbon nanotube experiment, gas atoms have been adsorbed in a 1D chain [2], and the chain's phonon frequencies have been predicted theoretically [3]. Experimental measurements of phonons in this physical system are lacking; therefore, experiments in another physical system are desirable. In the 1D colloidal experiment [1] the breathing and sloshing modes were measured, but other modes were not. Complete results have been reported for 2D lattices [4,5], but the modes are different in 1D.

Therefore, we note a broad interest in the oscillations of 1D chains, but a lack of complete experimental measurements, which we will provide in this paper. The experimental system we used is a dusty plasma, with charged micron-sized particles confined in a single row [6,7]. This type of confined 1D chain has the advantage of allowing direct imaging of particle positions and velocities, thereby allowing observations of the phonons. We also note other physical systems that consist of chains. In an ion storage ring, a 1D Coulomb chain has been formed, which might be used in atomic clocks [8] or quantum computing [9]. In magnetorheological suspensions, submicron magnetic particles dispersed in a nonmagnetic fluid interact through dipole moments aligning with an external magnetic field, forming dipolar chains [10]; these suspensions have commercial use for electronically controllable mechanical systems.

Here, we study phonons in a chain with a finite number  $N$  of charged particles, confined by a harmonic potential. Ex-

perimentally, we use a dusty plasma consisting of electrons, ions, neutral atoms, and small particles of solid matter. These so-called dust particles are polymer microspheres that acquire a negative charge and are confined as a 1D chain in an external potential well [7]. Theoretically, we model the chain as a single row of charged particles interacting with a Yukawa potential, moving in a horizontal plane and confined by a harmonic potential, in the presence of a damping that is proportional to particle velocity.

The chain in our experiment is a driven system. Particles undergo a fluctuating Brownian motion by colliding with gas atoms. In addition, the energy of these charged particles is increased by electrostatic fluctuations in the plasma, and it is dissipated by a frictional drag due to the gas [11]. In a steady state, the gain and the dissipation of energy are balanced.

The collective motions of particles can be treated as consisting of phonons, or modes, which in an experiment can arise two different ways. First, phonons naturally exist in a lattice that has a finite temperature [4,5], driven by spontaneous fluctuations. These motions can be decomposed as harmonic-oscillator-like modes, which we term natural phonons. Here we use the term "natural" to distinguish phonons that are present naturally from those that are deliberately excited by external manipulation. Natural phonons correspond to random particle motion; we would say that they correspond to thermal motion if our system were in thermal equilibrium. However, because our system is not in thermal equilibrium, we avoid calling the phonons "thermal" and instead use the more general term "natural."

Second, phonons can be excited in experiments by manipulations using external forces. Several experiments have been reported with *in situ* measurements of externally excited phonons in 1D [7] and 2D [12,13] dusty plasma crystals. In these experiments, phonons were continually stimulated at a specific frequency, making up a wave that propagated away from the excitation location. This wave has the same frequency as the excitation. Due to damping, the wave's amplitude decays as it propagates.

This paper presents experimental results and a model for phonons in a 1D chain. Section III presents experimental

\*Electronic address: bliu@newton.physics.uiowa.edu

†Electronic address: john-goree@uiowa.edu

results. We use a method of current autocorrelation functions (CAF) and the spectrum of the CAF to characterize the natural phonons, yielding the phonon spectrum and the temporal decay time of phonons.

Our two chief results are tests of energy equipartition and the dispersion relation. We observed that the phonon energy deviates from the equipartition law, indicating the existence of damping or heating mechanisms other than particle Brownian motion in a neutral gas medium. We found that, for the transverse mode, the dispersion relations for natural and externally excited phonons are not the same; in Sec. IV we explain the origin of this difference. Our experimental results presented here were recorded during the same experiment as in Ref. [7], except that in Ref. [7] a laser was used to excite phonons. Here we report data for natural phonons in the absence of any external manipulation. Our data, which were not previously reported, were recorded after recording data with external manipulation.

In Sec. IV, we develop a model to describe the phonons in a 1D dusty plasma chain. This model might also be applicable to 1D chains in colloids, storage rings, nanotubes, and other 1D systems. This model distinguishes how the phonons are excited. It yields dispersion relations for two cases: natural phonons and phonons excited by an externally applied sinusoidal force. For natural phonons, this model also yields a CAF and the spectrum of the CAF. All these results are suitable for direct comparison to the experiment.

Another model, which is also suitable for direct comparison to the experiment, was reported recently by Piacente, Peeters, and Betouras [14]. As in our model, that model begins with the equation of motion for a 1D chain and it yields dispersion relations like ours presented in Sec. IV. The model we develop in Sec. IV yields not only a dispersion relation, but also two other results that can be compared directly to experiment: a CAF and the spectrum of the CAF.

## II. EXPERIMENTAL METHOD

In the experimental setup, which is described in detail in Refs. [7,15], a plasma was produced in a capacitively coupled radio frequency (rf) discharge, using a 13.56 MHz rf voltage with a peak-to-peak amplitude of 94 V and a self-bias of  $-48$  V. Xenon gas was used at a low pressure of about 5 mtorr. A small number of melamine-formaldehyde microspheres were shaken into the plasma. These particles had a diameter of  $8.09 \pm 0.18 \mu\text{m}$  and a mass density of  $1.514 \text{ g/cm}^3$ . They gained a large electric charge due to exposure to the plasma, so that they were levitated by the electric field in the plasma sheath above a lower electrode.

We tracked particles from one frame to the next, calculating their velocities. This was done by illuminating them with a HeNe laser sheet and viewing them from above with a video camera at 29.97 frames per second, and a field of view of  $13 \times 10 \text{ mm}^2$ . Particle positions  $(x_i, y_i)$  were measured in each frame with subpixel spatial resolution, and velocities were calculated by subtracting the positions in consecutive frames. We then subtracted the center-of-mass velocity of the chain, yielding  $(\vec{v}_{x,i}, \vec{v}_{y,i})$ ; this subtraction has the effect of excluding the sloshing mode, which is a rigid-body motion of all particles in the confining potential.

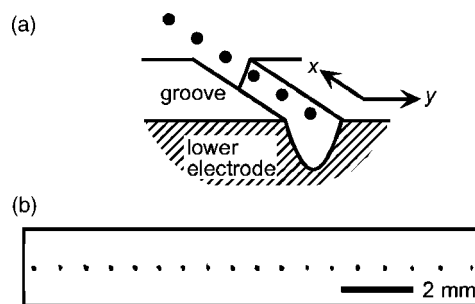


FIG. 1. (a) Sketch of a chain of particles levitated in a plasma sheath above a groove in the lower electrode of the apparatus. (b) Top view image of the central portion of a chain of length  $N=28$ .

Our 1D chain was externally confined by the natural electric fields in the sheath above the lower electrode. The sheath conforms to the shape of the electrode, which had a groove-shaped depression along the  $x$  direction. Everywhere along the groove's length, it had a parabolic shape in the  $y$  direction, Fig. 1(a). Because this groove was narrow, we formed a 1D chain, rather than a 2D [16] or 3D [17] suspension of particles in dusty plasmas.

Compared with a 2D dusty plasma crystal, our 1D chain has several differences. First, the equilibrium positions of particles do not change significantly with time, unlike in a 2D dusty plasma crystal, where the crystal might rotate. Second, the longitudinal and transverse modes do not significantly couple to each other, unlike in a 2D dusty plasma crystal, where pure shear or compressional modes do not exist due to the circular boundary of the crystal [5]. Third, the transverse mode in our 1D chain is a backward wave, with a frequency that decreases with wave number.

The experimental procedure, summarized below, was repeated for three different numbers of particles:  $N=10$ , 19, and 28. First, we introduced a single particle into the groove, and used the laser manipulation method of Ref. [15] to measure the confining potential. The particle motion was harmonic, indicating that the confining potential has a parabolic shape in all three directions, characterized by the frequencies  $\omega_x=2.6$ ,  $\omega_y=19.0$ , and  $\omega_z=94.2 \text{ s}^{-1}$  in the  $x$ ,  $y$ , and vertical directions, respectively. The high value of  $\omega_z$  shows that our confinement in the vertical direction is very strong, so that particle displacements from equilibrium positions are primarily 2D, in the horizontal plane. From the motion of a single particle, we also measured [7] the frictional damping rate,  $\nu=3.5 \text{ s}^{-1}$ .

Second, we introduced the desired number of additional particles, which self-assembled into a chain. Our camera's field of view included only the central portion of the chain, as shown in Fig. 1(b) for  $N=28$ , except that for our shortest chain,  $N=10$ , it included the entire chain. We recorded the data reported in Ref. [7] for phonons externally excited by the manipulation laser. Then, we turned the manipulation laser off, and after waiting 30 min to allow equilibration, we recorded 270 s of data. The average interparticle distance, for all particles in the field of view, was  $a=0.72$ , 0.8, and 1.25 mm for  $N=28$ , 19, and 10, respectively. The interparticle spacing was not uniform; it was 15% smaller in the center than at the chain's end, with a gradient of  $\partial a / \partial x \approx 0.01$ , for  $N=28$ .

Charged particles in this trap are believed to interact through a Yukawa potential,

$$\phi = \frac{Q^2}{4\pi\epsilon_0 r} e^{-r/\lambda_D}, \quad (1)$$

as demonstrated in Ref. [18] under similar conditions, for a monolayer of particles of charge  $Q$  levitated in a plane perpendicular to the ion flow. Tests with our apparatus are also consistent with a Yukawa potential [15]. The screening length  $\lambda_D$  is attributed to the free electrons and ions surrounding the particles.

We measured  $\lambda_D=0.86$  mm and  $Q=7600 e$ . As in Refs. [7,15], the value for  $\lambda_D$  was obtained using a method based on the equilibrium particle position; this method also yielded a range of values for  $Q$ . An additional method is required to determine  $Q$  accurately. Throughout this paper, as in Ref. [7], we use a value of  $Q$  that was found by fitting experimental data for an externally excited longitudinal wave to the corresponding theoretical dispersion relation, which will be presented in Sec. IV C.

In this experiment, we use the current autocorrelation function (CAF) and the spectrum of the CAF to characterize natural phonons. This is different from methods previously used in dusty plasma experiments: the Fourier spectra of the velocity field in Ref. [4] and the normal mode spectra in Ref. [5]. Both yielded a power spectrum of a collective current that was calculated directly from the velocity data without using a correlation function. Here, we first calculate the autocorrelation function of a collective current (CAF), yielding information in the time domain such as how spontaneous fluctuations decay with time. We then calculate the Fourier transform of the CAF, yielding spectra for various values of the wave number, which we combine to yield a phonon spectrum. For a stationary random process, according to the Wiener-Khinchine theorem, the power spectrum is equal to the Fourier transform of the autocorrelation function. Thus, our method provides information similar to the phonon spectrum as in Refs. [4,5], plus it also provides additional information in the time domain.

Correlation functions are used extensively in the analysis of noise and fluctuations of statistical systems [19], in theoretical analysis [20], and as a diagnostic for molecular-dynamics simulations [21]. For a Yukawa system intended to model dusty plasmas, correlation functions have been used in a theoretical study of the properties of 2D liquids [20]. Correlation functions can be computed from our experimental data, in the same way as from molecular-dynamics data, because our experiment provides the same measured results: particle position and velocity.

There are several methods that can be used to obtain a phonon spectrum. In most experimental systems, one uses x-ray or neutron scattering to measure a spectrum, and from this it is possible, if desired, to compute correlation functions. In our experimental system, direct imaging of particles yields a completely different kind of data to begin with: the positions and velocities of individual particles. With these data, we have a choice of either computing a spectrum directly as in Ref. [4], or computing the dynamic structure factor  $S(k, \omega)$  as in Ref. [20], or computing a current corre-

lation function and then Fourier transforming to yield a spectrum, as we do in this paper. The dynamic structure factor  $S(k, \omega)$  corresponds to a density autocorrelation function, and it is calculated based on particle position only. We computed  $S(k, \omega)$  for our experimental data, but we found that it was noisy, and in any case it provides data only for the longitudinal and not the transverse mode. We therefore must choose between the method of Ref. [4] and the method beginning with the CAF. We chose the latter because it offers a straightforward normalization of the energy units and because it yields correlation functions that have a low noise level, thereby allowing an accurate characterization of the decay rate of phonons. We note that the longitudinal CAF is related to  $S(k, \omega)$  by a continuity equation [20].

The current autocorrelation functions are

$$C_T(k, t) = \frac{1}{N} \langle j_T(k, t) j_T(-k, 0) \rangle \quad (2)$$

for the transverse mode and

$$C_L(k, t) = \frac{1}{N} \langle j_L(k, t) j_L(-k, 0) \rangle \quad (3)$$

for the longitudinal mode. We computed the correlation functions over a range  $0 \leq t \leq \tau$ , where we chose  $\tau=68.27$  s. Here  $k$  is the wave number, and the currents are defined as

$$j_T(k, t) = \sum_{i=1}^N \tilde{v}_{y,i}(t) e^{ikx_i(t)} \quad (4)$$

and

$$j_L(k, t) = \sum_{i=1}^N \tilde{v}_{x,i}(t) e^{ikx_i(t)}, \quad (5)$$

where  $N$  is the number of particles and  $i$  is an index for the particle number. In the experiment, if our camera field of view does not include all  $N$  particles in the chain, we replace  $N$  by the number of particles that we actually view.

As is common for MD simulations, we replace the ensemble average  $\langle \dots \rangle$  in Eqs. (2) and (3) with a time average over a finite interval [22,23]. The entire time series for a current  $j(k, t)$  is broken into  $M_t$  segments, each of duration  $\tau$ . Each segment, indexed by  $l_t$ , is started after a delay  $l_t \Delta t$ . It is common [22] to choose  $\Delta t < \tau$  so that the segments overlap in order to increase the number of segments  $M_t$  entering into the calculation of the average  $\langle \dots \rangle$ . We thus compute the correlation functions in Eqs. (2) and (3) as

$$C(k, t) = \frac{1}{NM_t} \sum_{l_t=0}^{M_t-1} j(k, t + l_t \Delta t) j(k, l_t \Delta t). \quad (6)$$

We chose  $\Delta t=1/\nu$ , the decay time due to gas damping. The entire time series had a duration  $M_t \Delta t=270$  s, which is much longer than the most important time scales for particle motion:  $1/\nu \approx 0.3$  s, and the period of a mode  $2\pi/\omega$ , which is  $\approx 2.4$  s for the slowest mode in our chain.

To verify that our time average yields a good ensemble average, we checked that CAF does not depend sensitively on the value of  $M_t$ . Repeating the calculation of Eqs. (2) and

(6) with five different intervals  $M_i \Delta t$  for the time series,  $M_i=200, 400, 600, 800,$  and  $900$ , we found that  $C_T(k, t)$  always looked like the same damped oscillation. To make the test quantitative, we verified that three parameters describing  $C_T(k, t)$  were essentially unchanged:  $C_T(k, 0)$ , the decay rate, and the oscillation frequency. These tests give us confidence that our averaging method yields a good ensemble average. Hereafter, we will always use  $M_i=900$ .

The spectra of the CAF are calculated using the Fourier transform of the CAF. For example, the spectrum of the CAF for the transverse mode is  $\tilde{C}_T(k, \omega) = 2\tau^{-1} \int_0^\tau C_T(k, t) e^{i\omega t} dt$ . This spectrum is calculated for a given value of  $k$ . Typically, we repeat the calculation of the spectra for various values of  $k$ .

### III. EXPERIMENTAL RESULTS

Here we report results recorded during the same experiment as in Ref. [7], except that in Ref. [7] a laser was used to excite phonons. Here we report data for natural phonons in the absence of any external manipulation; these data were not previously reported.

#### A. Time series

Particles in our chain were immersed in a neutral gas, which causes a particle to undergo Brownian motion. The particles might not be in thermal equilibrium, however, because they can also be accelerated by electrostatic fluctuations related to ion flow and the plasma sheath. The temperature  $T_p = \langle m\bar{v}_x^2 \rangle = \langle m\bar{v}_y^2 \rangle$ , as calculated from the time series for particle velocities, is  $0.02 \pm 0.01$  eV. Here  $m$  is the particle mass. As we mentioned earlier, we have subtracted the center-of-mass motion in obtaining this temperature; the actual particle energy was higher. The uncertainty  $\pm 0.01$  eV arises from random errors in particle position measurement. These errors prevent us from calculating a velocity distribution function, but they do not adversely affect the spectral methods we report next.

#### B. Current autocorrelation function (CAF)

Our chain exhibits harmonic-oscillator-like collective modes, i.e., natural phonons. On a time scale of 2 s, we observe a rapidly decaying phonon, as indicated by the damped oscillations in the CAF for the modes at  $k = 1.13 \text{ mm}^{-1}$ , shown in Figs. 2(a) and 2(c) for the transverse and longitudinal modes, respectively. To fit the first few damped oscillations, we use a damped harmonic-oscillator model of phonons in a chain,

$$C(k, t) = \frac{k_B T_p}{m} e^{-\nu_{fit} t/2} \left( \cos(\Omega_k t) + \frac{\nu_{fit}}{2\Omega_k} \sin(\Omega_k t) \right). \quad (7)$$

We will derive Eq. (7) in Sec. IV B. The oscillation frequency  $\Omega_k$  is related to the natural frequency  $\omega_k$  of an undamped phonon and the decay rate  $\nu_{fit}$  by  $\Omega_k^2 = \omega_k^2 - \nu_{fit}^2/4$ . We fit our results to Eq. (7), yielding values for  $\omega_k$ ,  $\nu_{fit}$ , and the temperature  $k_B T_p$ . For the transverse mode at  $k = 1.13 \text{ mm}^{-1}$ , we find  $\omega_k = 18.7 \text{ s}^{-1}$ ,  $\nu_{fit} = 5.0 \text{ s}^{-1}$ , and  $k_B T_p = 0.013$  eV.

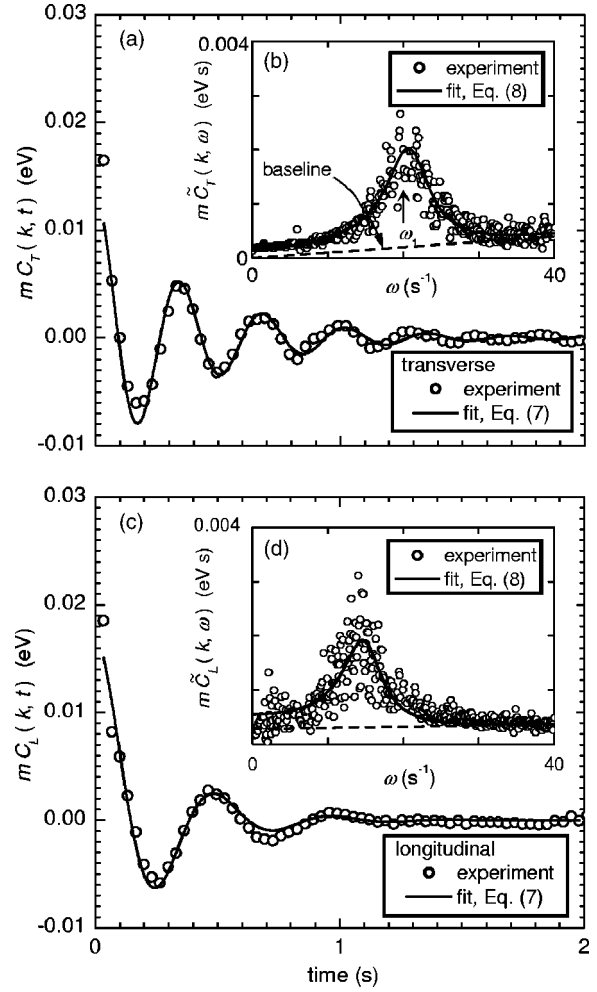


FIG. 2. (a) and (c) Current correlation functions (CAF). Both  $C_T(k, t)$  and  $C_L(k, t)$  exhibit damped oscillations. Here  $C_{T,L}(k, t)$  is computed from Eqs. (2) and (3) and then multiplied by the particle mass, giving it units of energy. (b) and (d) The spectra of the CAF. Most of the energy is concentrated around a peak at  $\omega_1$ . The experimental spectra  $\tilde{C}_{T,L}(k, \omega)$  are the Fourier transform of  $C_{T,L}(k, t)$ . The theoretical curve is a fit with three free parameters:  $\omega_1$  and  $\nu_{fit}$ , which yield one data point for the real and imaginary parts of the dispersion relation, respectively, as well as  $k_B T_p$ . Data shown are for the modes with  $k = 1.13 \text{ mm}^{-1}$ ; we measured the spectra of the CAF for other values of  $k$  also, to find the dispersion relations.

Similarly, for the longitudinal mode, at the same  $k$ , we find  $\omega_k = 14.2 \text{ s}^{-1}$ ,  $\nu_{fit} = 7.8 \text{ s}^{-1}$ , and  $k_B T_p = 0.017$  eV. The decay rate  $\nu_{fit}$  is of the order of the gas-damping coefficient,  $\nu = 3.5 \text{ s}^{-1}$ , indicating that natural phonons are significantly damped by gas drag.

#### C. Spectra of the CAF

Next, we Fourier transform  $C_T(k, t)$  and  $C_L(k, t)$ , for a given value of  $k$ , yielding the spectra of the CAF,  $\tilde{C}_T(k, \omega)$  and  $\tilde{C}_L(k, \omega)$ . We then subtract a sloping baseline, corresponding to instrumental noise, in  $\tilde{C}_T(k, \omega)$  and  $\tilde{C}_L(k, \omega)$ .

The sloping baseline is intended to account for instrumental noise in the particle velocity data. This noise arises as

follows. We calculate a particle's velocity as the difference in the particle's position in two consecutive frames. The position is determined from a camera image using the moment method [24] to find the center of the multiple pixel region corresponding to a particle. Each pixel has some randomly varying electronic noise, so that the pixel's brightness fluctuates, and this affects the calculated particle positions and therefore velocities. Empirically, we find that the effect of the random noise is to displace the spectrum upward, and this displacement is larger at higher frequencies. By modeling this displacement as a baseline, with two parameters, slope and intercept, we are able to fit the experimental spectrum. This method of correcting data for the instrumental noise in the frequency domain is much more effective than attempting to correct the data in the time domain. Consequently, the particle temperature computed using this spectral method is more precise than when computed from the time series.

Results for the spectra of the CAF are shown in Figs. 2(b) and 2(d). The spectra have most of their phonon energy concentrated in a frequency band centered around a peak at  $\omega_1$  with a linewidth  $\Delta\omega$ . The linewidth  $\Delta\omega$  is rather wide; for example in Fig. 2(b) for the transverse mode,  $\omega_1/\Delta\omega=3.3$ . Effects that contribute to  $\Delta\omega$  include damping of phonons by friction in the neutral gas, anharmonic effects, and the non-uniform particle spacing which has the effect of making the resonance frequency  $\omega_1$  not a single pure frequency.

We fit the experimental spectra to a model spectrum,

$$\tilde{C}(k, \omega) = \frac{\nu_{fit} k_B T_p}{m \pi} \frac{\omega_k^2}{(\omega^2 - \omega_k^2)^2 + (\omega \nu_{fit})^2}. \quad (8)$$

We will derive Eq. (8) in Sec. IV B. There are three free parameters in the fit:  $\omega_k$ ,  $\nu_{fit}$ , and  $k_B T_p$  describe the spectrum. This fit was our method of measuring  $\omega_1 \equiv \sqrt{\omega_k^2 - \nu_{fit}^2}/2$ , except for the portion of our longitudinal-mode data with  $ka < 0.5$ , where the fit was poor due to an extra peak at  $\omega \approx 2 \text{ s}^{-1}$ ; for that portion we measured  $\omega_1$  instead by finding the maximum of a smoothed spectrum. For Figs. 2(b) and 2(d), which show the spectra of the CAF computed for the modes at  $k=1.13 \text{ mm}^{-1}$ , fit results were as follows. For the transverse mode,  $\omega_1=20.1 \text{ s}^{-1}$ ,  $\nu_{fit}=6.2 \text{ s}^{-1}$ , and  $k_B T_p=0.016 \text{ eV}$ . For the longitudinal mode,  $\omega_1=15.0 \text{ s}^{-1}$ ,  $\nu_{fit}=8.2 \text{ s}^{-1}$ , and  $k_B T_p=0.018 \text{ eV}$ . Fitting the spectra of the CAF for all values of  $k$  (but excluding the longitudinal mode with  $ka < 0.5$ ) for three chains,  $N=10, 19$ , and  $28$ , yields an averaged value of  $k_B T_p$ , which is  $0.018 \text{ eV}$ , and  $\nu_{fit}=5.3 \text{ s}^{-1}$ .

The phonon decay rate is not one of chief experimental results, but it is useful to discuss the discrepancy between the measurement of the phonon decay rate  $\nu_{fit}=5.3 \text{ s}^{-1}$  for a 1D chain and the gas damping rate  $\nu=3.5 \text{ s}^{-1}$  for a single particle. This discrepancy is presumably due to interparticle interactions. Otherwise, if phonon decay is due to only gas damping, both measurements would yield the same results, because nothing was changed other than the number of particles. One type of interparticle interaction is an anharmonic effect arising from nonlinear terms in the interparticle interactions; such an effect causes a wave's frequency to change as it propagates along a chain. Other possible causes are the

nonuniform particle spacing and the finite chain length in the experiment. Whichever of these effects is largest, it nevertheless has a weaker effect than gas damping, because the frictional damping rate  $\nu=3.5 \text{ s}^{-1}$  accounts for more than half the observed decay rate  $\nu_{fit}=5.3 \text{ s}^{-1}$ .

#### D. Phonon spectrum

Combining the spectra of the CAF for all values of  $k$  yields a phonon spectrum. Results for the longitudinal and transverse modes are shown in Figs. 3(a) and 3(b) for  $N=28$ . The vertical axis is the phonon energy in a frequency band  $\delta\omega=2\pi/\tau$ , i.e.,  $m\tilde{C}_T(k, \omega)\delta\omega$  and  $m\tilde{C}_L(k, \omega)\delta\omega$  for transverse and longitudinal modes, respectively. The values of  $k$  were chosen as  $k=s\pi/L_x$ , where  $s=1, 2, \dots$ . Here,  $L_x$  is the distance between the two outer particles that were included in the image. The maximum value of  $s$  was the number of particles we viewed minus two; it was less than  $N$  for two reasons. First, for  $N=19$  and  $28$  our camera's field of view did not include every particle. Second, we excluded the sloshing mode,  $s=0$ .

Here, we chose values of  $k$  that are equally spaced; our motivation for this choice is that it is convenient, and that there is no unique choice for the wave number  $k$  for each mode, because the  $N$  modes for  $N$  particles overlap in wave-number space. In Ref. [7], we reported a lack of reflected waves from the chain's end, as observed in the chain's center where we make our measurements, for an experiment with externally excited waves. In the absence of such reflections, we cannot expect to distinguish one mode from another. In wave-number space, each mode has a finite width, overlapping with the next mode. For these reasons, it is acceptable to perform a Fourier analysis assuming modes of the form  $e^{ikx}$ , even though the chain is finite and the particle spacing is not regular. Another method, which would also be acceptable, would be a normal-mode analysis [5], which results in a spectrum where the horizontal axis has a depiction of discrete mode numbers rather than a continuous varying wave number  $k$ .

One of our chief results is that the observed phonon spectrum is broadband, and its energy is not partitioned equally among modes.

The phonon spectrum is broadband in frequency. Our time series included 2048 frames, so that our measured frequency spectrum was computed for a correspondingly large number of frequencies. We find that our observed spectrum is smooth, not consisting of  $\delta$  functions, and it has a finite linewidth. The largest contribution to this linewidth is phonon decay arising from gas friction.

The energy in the phonon spectrum in our experiment was not equally partitioned among phonon modes; instead, it was somewhat concentrated at smaller values of  $k$ . For the longitudinal mode, this is seen in Fig. 3(c), which is a graph of the phonon energy distribution versus wave number. This graph was computed by integrating the phonon spectrum in Fig. 3(a) over frequency. Note the peak at small  $k \approx 0.5 \text{ mm}^{-1}$ , corresponding to a wavelength of  $\approx 13 \text{ mm}$ , which is of the same order as the  $20 \text{ mm}$  length of the  $N=28$  chain. There would be a similar peak for the transverse mode if we did not

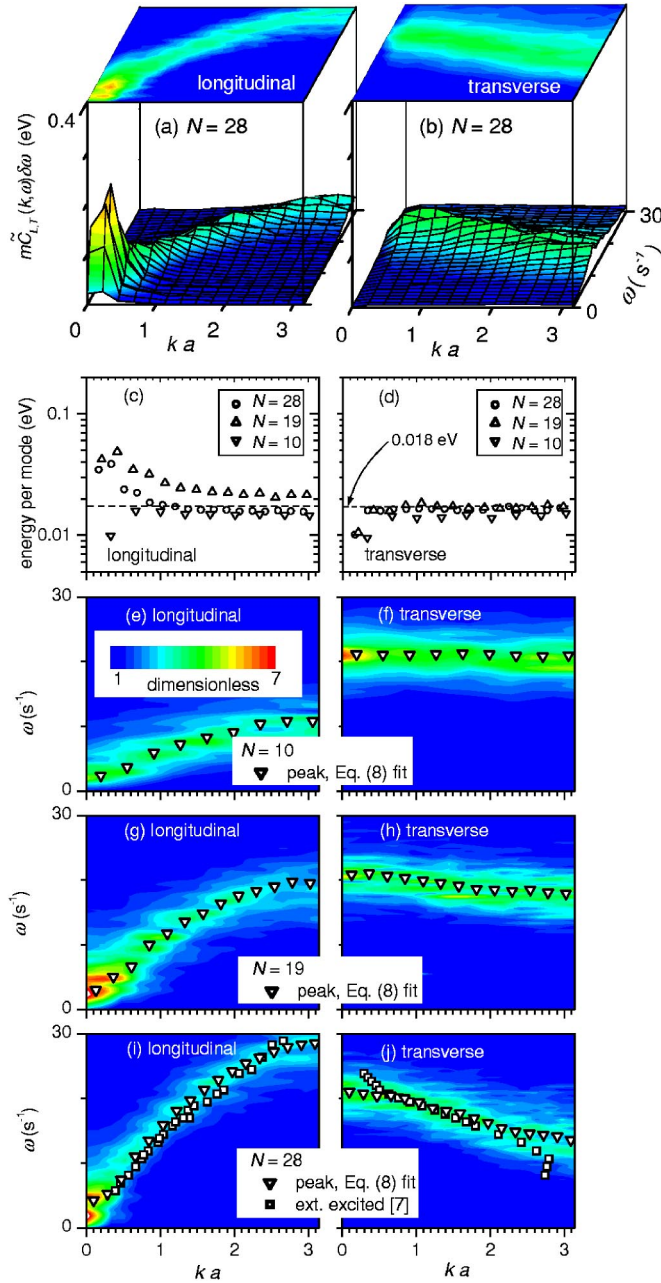


FIG. 3. (a), (b) Phonon spectrum, made by combining the spectra of the CAF as in Figs. 2(b) and 2(d) for various  $k$ . (c), (d) Phonon energy variation with wave number, computed by integrating the data in (a) and (b) over  $\omega$ . In (c), note the concentration of phonon energy at long wavelengths, indicating a lack of equipartition. (e)–(j) Normalized phonon spectra, computed by normalizing the color separately for each value of  $k$ , as in (a) and (b), by the energy per mode as in (c) and (d). Note that the experimental dispersion relation for natural phonons (triangles) differs from that for externally excited phonons (squares).

subtract the center-of-mass motion. This result is different from earlier observations in a 2D dusty plasma crystal [4], where the phonon energy was almost equally distributed with respect to wave number. Our observation of a lack of equipartition offers a clue to some unexplored problems in the physics of dusty plasmas, which we discuss next.

We can propose a possible reason for the deviation from energy equipartition. The heating mechanism [25], which includes both Brownian motion due to collisions with gas atoms and electrostatic fluctuations, might favor depositing energy into long-wavelength phonons, if, for example, the heating mechanism intrinsically has low frequencies. We note that the experimental spectrum in Fig. 2(d) has an additional peak at  $\omega \approx 2 \text{ s}^{-1}$ . We speculate this peak is coherent noise due to low-frequency ( $\omega \approx 2 \text{ s}^{-1}$ ) fluctuations present in the plasma, although we made no other measurements to observe such fluctuations. This possibility requires further study.

Another measurement of  $k_B T_p$ , in addition to those we have presented using the time series and the spectra of the CAF, can be obtained by averaging the phonon energy for all wave numbers. We do this by averaging all the data points in Figs. 3(c) and 3(d). This result, 0.018 eV, matches both the value from fitting the spectra and the less precise value from the time series. We note that all three results exclude the sloshing mode's energy, because we removed the center-of-mass motion as the first step in our data analysis. Therefore, there is no reason that our measurements must yield a temperature greater than room temperature, 0.025 eV.

### E. Dispersion relation

To reveal the dispersion relations for the longitudinal and transverse modes, we prepared Figs. 3(e)–3(j), which were computed by normalizing the color separately for each value of  $k$ . This was done by normalizing the spectra of the CAF for each value of  $k$ . The denominator is the same quantity plotted in Figs. 3(c) and 3(d). We did this normalization separately for the longitudinal and transverse modes. This yields plots of the phonon spectrum as if energy were partitioned equally among the modes. This “normalized phonon spectrum” allows the viewer to easily see the dispersion relation. The data for the normalized phonon spectra shown in Figs. 3(e)–3(j) include the first Brillouin zone. Also shown with the normalized phonon spectra are triangle symbols representing the value of the peak frequency  $\omega_1$ ; these symbols are our experimental measurement of the dispersion relation of natural phonons.

Examining the dispersion relations, we can identify features that we attribute to the confining potential, the value of  $\kappa = a/\lambda_D$ , and the role of gas friction. We will examine each of these three effects next.

Due to the confining potential in the  $y$  direction, the transverse mode has a frequency that decreases with wave number, i.e., it is a backward wave. This is different from the dispersion relation of transverse phonons in a 2D dusty plasma crystal, where the transverse wave is forward, i.e., its frequency increases with wave number [4].

Due to the confining potential in the  $x$  direction, the longitudinal mode has a minimum nonzero frequency as  $k \rightarrow 0$ . This minimum frequency corresponds to the longitudinal sloshing mode. A minimum frequency should also occur in a 2D dusty plasma crystal, for the same reason as in 1D, although the authors of Ref. [4] for a 2D experiment did not comment on this observation. Unlike the transverse mode,

the longitudinal mode is forward, because the restoring force for a particle arises mainly from interparticle interactions rather than the confining potential.

The effect of varying  $\kappa$  is a change in the slope of the dispersion relation. This slope is steeper for larger  $N$ , for both the longitudinal and transverse modes. This is due primarily to a greater compression [15] of the chain's center as particles are added to the end of the chain, where the confining forces are larger along the  $x$  axis. As the chain is compressed,  $a$  and  $\kappa$  are reduced and  $\Gamma = Q^2/4\pi\epsilon_0 a k_B T_p$  becomes larger. These trends can be seen in our parameters. As  $N$  was increased from 10 to 19 and then 28,  $\Gamma$  increased from 3325 to 5195 and then 5772, while  $\kappa$  decreased from 1.45 to 0.93 and then 0.84.

Another of our chief results is that there is a difference in the dispersion relation for natural and externally excited phonons, visible in our data for the transverse mode, which we attribute to the role of gas friction. This difference is prominent at the smallest and largest values of  $k$  in Fig. 3(j). We are unable to say whether the longitudinal mode has a similar difference, because we lack data for externally excited longitudinal modes at small and large  $k$ , due to our method of excitation. We will develop a model in Sec. IV to account for the difference between the dispersion relations of natural and externally excited phonons. This model will reveal that gas friction accounts for the observed difference, as explained in Sec. V.

#### IV. MODEL

Here we develop a model describing phonons in a 1D chain. This model is different from previous models [3,26–29] in two respects. First, it distinguishes how the phonons are excited and yields dispersion relations for two cases: natural phonons and phonons excited by an externally applied sinusoidal force. Second, it yields a CAF and the spectrum of the CAF for natural phonons, which are suitable for direct comparison with the experiment.

##### A. Equation of motion of a 1D chain

The physical system we model has identical charged spherical or pointlike particles that interact through a Yukawa potential. The particles are limited in their motion to a horizontal plane, where they are confined in a single row by a harmonic potential in the transverse direction. Particles are uniformly spaced. The particle motion is damped by a frictional force corresponding to gas drag. Motion is also excited by a force that varies randomly in direction and time, corresponding to Brownian motion for a particle in thermal equilibrium with a gas. However, we do not include a random force for the case of externally excited phonons. To allow a comparison to experiments that have a weak confining potential in the longitudinal direction in addition to the required harmonic potential in the transverse direction, we include a harmonic potential in the longitudinal direction, characterized by a nonzero  $\omega_x$ .

The reader may set the parameter  $\omega_x$  to zero to obtain results that are fully consistent with the assumption of uni-

form spacing. A nonzero  $\omega_x$  introduces an inconsistency with our assumption that the particle spacing is uniform, but this inconsistency can be insignificant. In Sec. V A, we compare the ratio of the decay length of a longitudinal sound wave in the presence of damping and the length scale for any gradient in the interparticle spacing. When this ratio is small, as it is for the experiment [7], the inconsistency is insignificant and our model can be applied locally to a portion of an infinite chain.

We consider the equation of motion for a single particle, including the following forces. The interparticle force is computed by including a particle's  $2M$  nearest neighbors. Assuming a small amplitude of particle displacement, we linearize this force with regard to a particle's displacement, thereby neglecting any anharmonic effects. The confinement force is characterized by a harmonic potential with spring constants  $m\omega_x^2$  and  $m\omega_y^2$  in the longitudinal and transverse directions, respectively. The frictional drag force is proportional to particle velocity,  $\nu_{fit}m\dot{x}_n$ , where  $\nu_{fit}$  is a theoretical damping rate, which can be computed using the Epstein drag model [11] for a microsphere moving through a rarefied gas. The random force  $\eta_n(t)$  can be due to any kind of fluctuations; it randomly couples energy to the particle. Finally, if desired, an externally applied force  $F_E(t)$  can be included.

Including all the forces listed above, the equation of motion of a particle is

$$m\ddot{x}_n = \sum_{l=1}^M K_{x,l}(x_{n+l} + x_{n-l} - 2x_n) - m\omega_x^2 x_n + F_E(t) - \nu_{fit}m\dot{x}_n + \eta_n(t) \quad (9)$$

for the longitudinal mode, and similarly for the transverse mode by substituting  $y_n$ ,  $-K_{y,l}$ , and  $\omega_y$  for  $x_n$ ,  $K_{x,l}$ , and  $\omega_x$ , respectively. Here, we have assumed that the equilibrium positions of all the particles lie on a common axis. Equation (9) is for particle  $n$ , which interacts with  $M$  neighbors on each side, i.e., the neighbors that have an index from  $n-M$  to  $n+M$ . In this paper, we treat two cases: a three-particle model, where a particle  $n$  interacts only with one immediate neighbor on each side, corresponding to  $M=1$ , and a five-particle model, where a particle  $n$  interacts with two neighbors on each side, corresponding to  $M=2$ .

The spring constants  $K_{x,l}$  and  $K_{y,l}$  in Eq. (9) depend on the particular physical system. Here we will assume a Yukawa potential, although the reader could use our model for other potentials simply by substituting an appropriate expression for the spring constants. Calculating the interparticle force based on Eq. (1) with equally spaced particles, and then linearizing for small amplitudes, yields the spring constants

$$K_{x,l} = \frac{Q^2(l^2\kappa^2 + 2l\kappa + 2)}{4\pi\epsilon_0 l^3 a^3 e^{l\kappa}}, \quad (10)$$

$$K_{y,l} = \frac{Q^2(1 + l\kappa)}{4\pi\epsilon_0 l^3 a^3 e^{l\kappa}} \quad (11)$$

for a Yukawa interaction between a particle and its neighbor at a distance  $la$ .

### B. Natural phonons

In this section, we will model the natural phonons as damped harmonic oscillators, which are abstract representations of collective particle motion.

In the absence of an external force  $F_E$ , Eq. (9) becomes

$$m\ddot{x}_n = \sum_{l=1}^M K_{x,l}(x_{n+l} + x_{n-l} - 2x_n) - m\omega_x^2 x_n - \nu_{fit} m \dot{x}_n + \eta_n(t) \quad (12)$$

for the longitudinal mode. A similar expression can be written for the transverse mode.

Applying a discrete spatial Fourier transformation to Eq. (12) yields

$$\ddot{Q}_k(t) + \omega_k^2 Q_k(t) + \nu_{fit} \dot{Q}_k(t) = \frac{\eta_k(t)}{m} \quad (13)$$

for every wave number  $k$ . Here,  $Q_k(t) = \sum_n x_n(t) e^{-ikna} / \sqrt{N}$  for the longitudinal mode; for the transverse mode one should substitute  $y_n(t)$  for  $x_n(t)$ . The natural frequency  $\omega_k$  is

$$\omega_k^2 = \omega_x^2 + \sum_{l=1}^M \frac{4K_{x,l}}{m} \sin^2 \frac{lka}{2} \quad (14)$$

for the longitudinal mode, and

$$\omega_k^2 = \omega_y^2 - \sum_{l=1}^M \frac{4K_{y,l}}{m} \sin^2 \frac{lka}{2} \quad (15)$$

for the transverse mode. In Eq. (13),  $\eta_k(t)$  is the Fourier transform of the random force,  $\eta_k(t) = \sum_n \eta_n(t) e^{-ikna} / \sqrt{N}$ .

In Eq. (13), the allowed values of the wave number  $k$  are determined by the length of the chain. For a chain of  $N$  particles,  $k$  has  $N$  discrete values. If we assume that the chain is infinite, i.e.,  $N \rightarrow \infty$ ,  $k$  can have any value. This assumption should not prevent us from comparing our model with a chain of finite length, because the discrete modes of a finite chain are points along the same dispersion relation curve as for an infinite chain.

Fourier transforming Eq. (13) yields

$$(-\omega^2 + \omega_k^2 - i\nu_{fit}\omega)Q_k(\omega) = \frac{\eta_k(\omega)}{m}, \quad (16)$$

where  $Q_k(\omega)$  and  $\eta_k(\omega)$  are Fourier transformations of  $Q_k(t)$  and  $\eta_k(t)$ , respectively. Equation (16) will be used to obtain first a dispersion relation and then a power spectrum.

First, we obtain the dispersion relation

$$\omega = \omega_r + i\omega_i = \sqrt{\omega_k^2 - \frac{\nu_{fit}^2}{4}} - i\frac{\nu_{fit}}{2}, \quad (17)$$

where the frequency  $\omega$  is a complex number. Note that in the real part, the frequency of the peak is shifted downward from  $\omega_k$  by the offset of damping.

Second, the power spectrum  $\tilde{C}(k, \omega)$  is calculated using  $\tilde{C}(k, \omega) = \omega_k^2 |Q_k(\omega)|^2$ , where  $\omega$  is a real number. The final form of the spectrum is

$$\tilde{C}(k, \omega) = \frac{\eta_k^2(\omega)}{m^2} \frac{\omega_k^2}{(\omega^2 - \omega_k^2)^2 + (\omega\nu_{fit})^2}. \quad (18)$$

The spectrum has a peak at  $\omega_1 \equiv \sqrt{\omega_k^2 - \nu_{fit}^2/2}$ , with a linewidth  $\Delta\omega$ . We define the linewidth  $\Delta\omega$  as the full width at half maximum of the peak, with  $(\Delta\omega/\omega_1)^2 = 2 - 2(1 - \nu_{fit}^2/\omega_1^2 - \nu_{fit}^4/4\omega_1^4)^{1/2}$ . The amplitude of the spectrum is determined by  $\eta_k(\omega)$ . For a chain of particles that are in thermal equilibrium with an ambient gas,  $\eta_k^2(\omega) = m\nu_{fit}k_B T_p / \pi$ .

Fourier transforming Eq. (18) to the time domain yields a corresponding current autocorrelation function (CAF)  $C(k, t)$ . For a system that is in thermal equilibrium, we obtain a model CAF

$$C(k, t) = \frac{k_B T_p}{m} e^{-\nu_{fit}t/2} \left( \cos(\Omega_k t) + \frac{\nu_{fit}}{2\Omega_k} \sin(\Omega_k t) \right), \quad (19)$$

which applies separately for each mode. From Eq. (19), the CAF exhibits damped oscillations, with a frequency of  $\Omega_k = (\omega_k^2 - \nu_{fit}^2/4)^{1/2}$  and a decay rate of  $\nu_{fit}/2$ .

### C. Phonons excited by an external sinusoidal manipulation

In this section, we consider phonons excited by an externally applied sinusoidal force. Here, we only consider the longitudinal mode. For the transverse mode, the corresponding model and experimental results were presented in Ref. [7].

We assume that a sinusoidal force, with a frequency  $\Omega$ , is applied only to a single particle, as it was in the experiment of Ref. [7]. We label this particle as  $n=0$ . The phonons that are excited will have the same frequency as the excitation frequency  $\Omega$ . Phonons are continually excited, making up a wave in the chain that propagates in both directions away from the excitation location.

The frequency of this externally excited wave is real, because the amplitude of the externally applied force remains constant with time. The wave number, however, is complex. When the wave is excited at a specific location using an externally applied force, the wave propagates away from the excitation location and its amplitude decays with distance, accounting for the imaginary part of the wave number. We note that this situation for an externally excited wave is different from that of natural phonons, which are commonly modeled with a complex frequency and a real wave number.

The motions of particles can be described by Eq. (12), except for particle  $n=0$ . The motion of particle  $n=0$  is primarily determined by the external force  $F_E \propto \cos \Omega t$ , so that its velocity is

$$\dot{x}_0 = A \sin \Omega t, \quad (20)$$

where  $\Omega$  is the known frequency of the excitation. We use the symbol  $\Omega$  to distinguish this case from that of the natural phonons.

Here, we solve Eq. (12), but with the boundary condition given by Eq. (20). We assume that the solution has the form  $x_n = B \exp[i(\Omega t - nka)]$ , where  $B = -A/\Omega$ , determined by the boundary condition Eq. (20). Thus, Eq. (12) is transformed to

$$\left( i\Omega\nu_{fit} - \Omega^2 + \sum_{l=1}^M \frac{K_{x,l}}{m} (2 - e^{-ik_l a} - e^{ik_l a}) + \omega_x^2 \right) B = 0, \quad (21)$$

where we have neglected the random force  $\eta_n(t)$ , as is appropriate if the external force is large,  $F_E(t) \gg \eta_n(t)$ .

The wave dispersion relation is determined from Eq. (21). As discussed above, the frequency  $\Omega$  is real, and the wave number is a complex number  $k = k_r + ik_i$ . We obtain the dispersion relation by numerically solving these two equations, which are functions of  $\Omega$ ,  $k_r$ , and  $k_i$ ,

$$\Omega^2 = \omega_x^2 + \sum_{l=1}^M \frac{2K_{x,l}}{m} (1 - \cos k_r l a \cosh k_i l a), \quad (22)$$

$$\Omega = \sum_{l=1}^M \frac{2K_{x,l}}{m\nu_{fit}} \sin k_r l a \cosh k_i l a. \quad (23)$$

## V. COMPARISON OF MODEL WITH EXPERIMENT

### A. Criterion for validity of the $\omega_x \neq 0$ assumption

As was mentioned in Sec. IV A, when our model is used with a nonzero value of  $\omega_x$  for the longitudinal confining potential, we must check a criterion for the validity of the assumption. To do this, we compare two distances: the decay length  $C_s/\nu$  for a propagating sound wave, and the length scale  $a(\partial a/\partial x)^{-1}$  for the gradient in the interparticle spacing. The longitudinal sound speed  $C_s = \partial\omega/\partial k$  was approximately  $11 \text{ mm s}^{-1}$  in the experiment, based on Fig. 3(i). We then calculate the distance traveled by a sound wave before it is damped significantly, yielding  $C_s/\nu \approx 3 \text{ mm}$ . For comparison, the gradient scale length  $a(\partial a/\partial x)^{-1}$  was approximately  $70 \text{ mm}$ . The ratio of these two distances is small,  $0.04$ . Thus, the criterion for the validity of assuming  $\omega_x \neq 0$  is satisfied, and our model can be locally applied to a portion of chain in our experiment. Here, we apply the model to the central portion of the chain  $N=28$ , comprised of the 18 particles that were imaged in the experiment.

### B. Phonons excited by external sinusoidal manipulation

As we reported in a previous paper [7], the dispersion relation can also be measured for externally excited waves. This was done by launching a wave at the midpoint of the chain by pushing it transversely at a specified real frequency. Waves propagating outward from the point of excitation were measured, using a Fourier-transform technique, yielding a complex wave number. In this way, we measured the real and imaginary dispersion relation. The externally excited waves are not translationally invariant, unlike the natural phonons. To analyze natural phonons, we use a correlation function CAF that is translationally invariant. The external excitation method did not employ any correlation functions in its analysis.

The theoretical dispersion relation exhibits the same trend as in the experiment with external excitation, i.e., the longi-

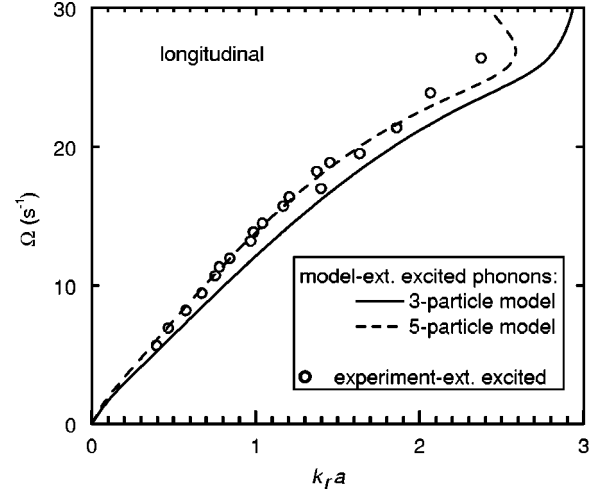


FIG. 4. Dispersion relation for externally excited longitudinal phonons. The frequency is real, and the wave number is complex. Dissipation is the cause for a nonzero value of  $k_i$ , and it might also affect the curve for  $k_r$ , shown here. In this experiment, we measured the real part of the longitudinal mode's wave number, shown here, by manipulating a particle to excite a sinusoidal wave. The charge  $Q$  used throughout this paper was measured by fitting the experimental data to the model with a five-particle model, Eqs. (22) and (23), with  $M=2$ .

tudinal mode is a forward wave. Only the real part of the dispersion relation is shown in Fig. 4. We were unable to measure the imaginary part of  $k$  because the wave was too weak to accurately measure the scale length of its exponential decay. Figure 4 shows the longitudinal mode's dispersion relation; the corresponding dispersion relation for the transverse mode, including the experiment and model, was presented in Ref. [7].

We find the charge  $Q$  by fitting the experimental dispersion relation to the five-particle model. This was the only free parameter in the fit. Other parameters used were  $\lambda_D$  and  $a$ , which were obtained from the equilibrium position [15]. The resulting value,  $Q=7600e$ , was used throughout this paper as the experimental measurement of  $Q$ .

### C. Natural phonons

The model CAF Eq. (19) is compared to experiment in Figs. 2(a) and 2(c), for the modes at  $k=1.13 \text{ mm}^{-1}$ . The theoretical curve in Figs. 2(a) and 2(c) is a fit using Eq. (19), with three free parameters, as mentioned in Sec. III. We find that the CAF for the experimental data and the model fit reasonably well. Both of them exhibit a damped oscillation. This indicates that a phonon in the experiment can be modeled as a damped harmonic oscillator.

The model spectra of the CAF are compared to experiment in Figs. 2(b) and 2(d), by fitting the experimental data points to the theoretical curve Eq. (18). In fitting the data, we first subtract a sloping baseline, as discussed in Sec. III. The example shown is for the modes at  $k=1.13 \text{ mm}^{-1}$ . The fit is good enough to yield useful values for  $\nu_{fit}$  and  $k_B T_p$ , as discussed in Sec. III.

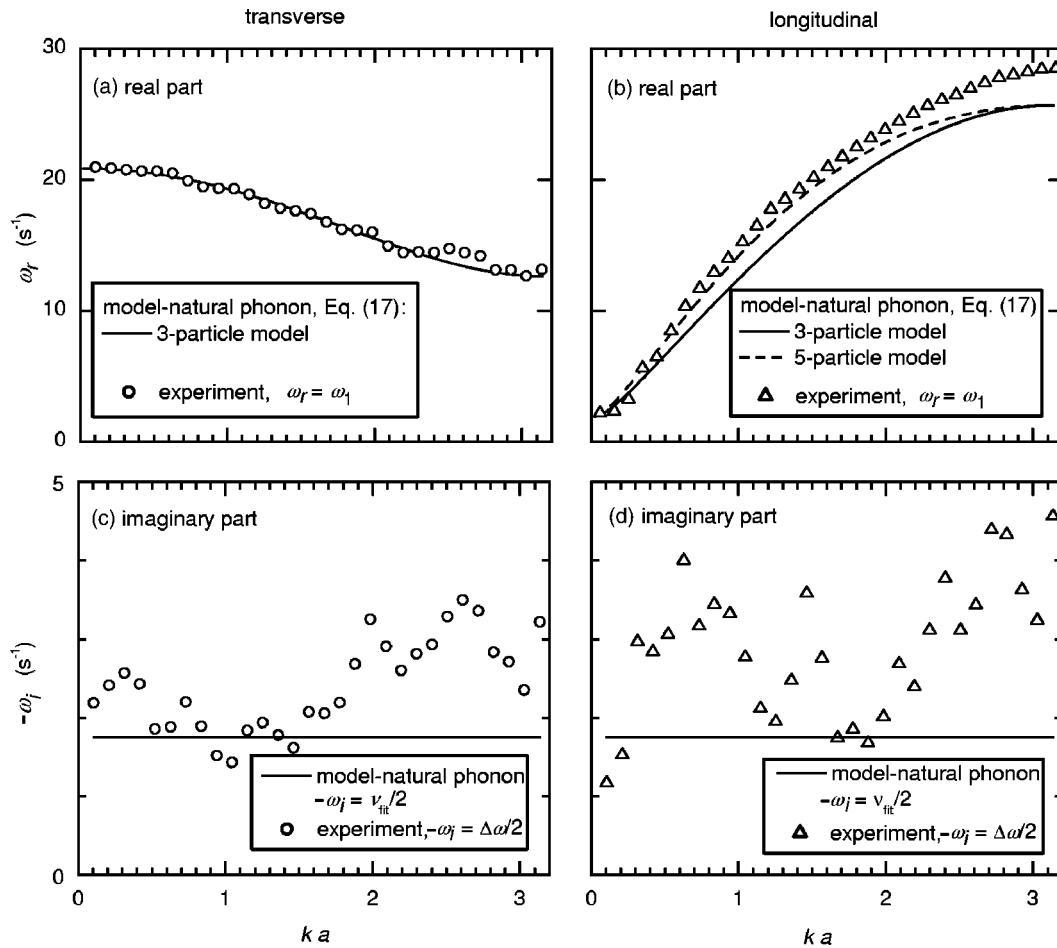


FIG. 5. Dispersion relation for natural phonons. The frequency is a complex number, and the wave number is real. Theoretical curves for the real and imaginary parts of  $\omega$  were computed from Eq. (17), with no free parameters. The experimental data points were obtained from the spectra of the CAF; for each value of  $k$ , we determined the peak  $\omega_1$  and the linewidth  $\Delta\omega$  of the spectra of the CAF, yielding  $\omega_r$  and  $\omega_i$ , respectively. Dissipation, for example due to gas damping, is the cause of a nonzero value of  $\omega_i$ . In the model, we used experimental values of  $a$  and  $\lambda_D$  obtained from equilibrium particle positions and a value of  $Q$  obtained by fitting separate experimental results of the dispersion relation for externally excited waves.

Finally, we test theoretical dispersion relations for both longitudinal and transverse modes, Fig. 5. Both the real and imaginary parts of the dispersion relation are shown in Fig. 5. The data shown for the real part of the experimental dispersion relations are the same as the triangle symbols in Figs. 3(i) and 3(j). The imaginary part of the dispersion relation is the variation of  $\omega_i$  with wave number  $k$ , shown in Figs. 5(c) and 5(d). For the experimental data,  $\omega_i$  was calculated from the measured linewidth  $\Delta\omega$  as  $\omega_i = -\Delta\omega/2$ . In the theoretical dispersion relations,  $\omega_r$  and  $\omega_i$  were calculated from Eq. (17).

For the transverse mode, the real parts of theoretical and experimental dispersion relations agree well, as seen in Fig. 5(a). The agreement is good even for the three-particle model ( $M=1$ ).

For the longitudinal mode, the real parts of theoretical and experimental dispersion relations agree roughly, when a three-particle model is used in the model, as seen in Fig. 5(b). This agreement is improved by using a five-particle model ( $M=2$ ).

For both the longitudinal and transverse modes, the theoretical imaginary part,  $\omega_i = -\nu_{fit}/2$ , is independent of wave

number  $k$ . In using this expression to calculate  $\omega_i$ , for  $\nu_{fit}$  we used the experimental value  $\nu = 3.5 \text{ s}^{-1}$ , which was obtained using a single particle. Results are shown in Figs. 5(c) and 5(d). Theoretical and experimental values of the imaginary part agree roughly. The experimental values, although they have some scatter, are mostly larger than the model assuming the single-particle damping rate.

#### D. The difference between natural and externally excited phonon dispersion relations

As we demonstrated experimentally in Sec. III, the real part of the dispersion relation  $\omega_r$  versus  $k$  for natural phonons is different from that for externally excited phonons. This is different from the result that would be expected in the absence of any dissipation; in that case, the dispersion relations would be purely real, and they would be the same regardless of the excitation mechanism. The role of dissipation, such as frictional gas damping in our experiment, is twofold. First, dissipation is responsible for an imaginary part. This imaginary part is different for natural and externally excited

phonons: as discussed in the previous section, for natural phonons  $\omega$  is complex and  $k$  is real, while for the externally excited phonons in our experiment  $\omega$  is real and  $k$  is complex. Second, dissipation also affects the real part of the dispersion relation. For natural phonons, this produces a downward shift in the real frequency  $\omega_r$  of the peak of the spectra of the CAF, as we discussed in Sec. IV, where we presented Eq. (17).

## VI. CONCLUSION

Experimental results and a model for a 1D chain were presented. Phonons were observed for a 1D chain of charged microspheres, levitated in a plasma above a groove in an electrode. A model was developed to describe the phonons in a 1D chain; this model might also be applicable to 1D chains in colloids, storage rings, nanotubes, and other 1D systems, in addition to our dusty plasma.

The phonon spectrum is broadband and characterized by a dispersion relation. The longitudinal mode is a forward wave; however, the transverse mode is a backward wave, with a frequency that decreases with wave number, due to the confining potential. The confining potential also affects the longitudinal mode; it cannot have a zero frequency, but instead has a nonzero frequency corresponding to the sloshing mode.

In this paper, we primarily report results for phonons corresponding to random particle motion, in the absence of external manipulation. We term these natural phonons to distinguish them from externally excited phonons, which were studied experimentally and theoretically in Ref. [7]. To characterize natural phonons, we used the current correlation function (CAF) and the spectrum of the CAF. We compute the spectra of the CAF for various values of the wave number, and combine them to yield a phonon spectrum. From the phonon spectrum, we can determine how energy is partitioned among modes. We also found the temporal decay of phonons two ways: from the decay time of the CAF and the linewidth of the spectra of the CAF.

Our two surprising experimental results for the phonon spectrum and dispersion relation are a lack of energy equipartition and a dispersion relation that is different from what was previously reported. First, the phonon energy is not par-

tioned equally among phonon modes. Instead, it is concentrated in the longest wavelengths. This result offers a hint that may be useful for gaining an understanding of an unexplained phenomenon: how particles in a monolayer dusty plasma can be heated beyond the temperature expected for Brownian motion, as was reported in Ref. [4]. Second, in the presence of frictional gas damping, the dispersion relation is different for externally excited and natural phonons. This difference is seen most strongly at small and large wave numbers.

A model was developed for a 1D chain interacting via the Yukawa potential. This model takes into account gas friction and distinguishes how phonons are excited. Dispersion relations were obtained for phonons excited by an externally applied sinusoidal force, and for phonons corresponding to random particle motion. For the latter case, we also obtained a CAF and the spectrum of the CAF. These theoretical results allow a direct comparison to our experiment.

To compare the model and our experiment requires three parameters:  $a$ ,  $\lambda_D$ , and  $Q$ . We obtained  $a$  and  $\lambda_D$  directly from the experimental data. We obtained  $Q$  by fitting the experimental dispersion relation to the model for an externally excited longitudinal phonon. After choosing these parameters, we can then test the dispersion relation for natural phonons using no free parameters.

For natural phonons, calculating the dispersion relation with no free parameters, we found that it agrees well with the experiment for the transverse mode. For the longitudinal mode with our value of  $\kappa$ , we find that agreement with experiment requires including a five-particle interaction, not just three.

We also compared the model and experimental CAF and the spectrum of the CAF. In these comparisons there were three free parameters (a mode's amplitude, frequency, and damping rate). A good fit to the experiment was achieved, indicating that the model's assumption of damped harmonic oscillators is suitable for describing the natural phonons in our 1D chain in the presence of damping.

## ACKNOWLEDGMENTS

We thank V. Nosenko and F. Skiff for helpful discussions. This work was supported by NASA and DOE.

- 
- [1] S. A. Tatarkova, A. E. Carruthers, and K. Dholakia, *Phys. Rev. Lett.* **89**, 283901 (2002).
  - [2] S. Talapatra and A. D. Migone, *Phys. Rev. Lett.* **87**, 206106 (2001).
  - [3] M. T. Cvitas and A. Siber, *Phys. Rev. B* **67**, 193401 (2003).
  - [4] S. Nunomura *et al.*, *Phys. Rev. Lett.* **89**, 035001 (2002).
  - [5] A. Melzer, *Phys. Rev. E* **67**, 016411 (2003).
  - [6] A. Homann, A. Melzer, S. Peters, and A. Piel, *Phys. Rev. E* **56**, 7138 (1997).
  - [7] B. Liu, K. Avinash, and J. Goree, *Phys. Rev. Lett.* **91**, 255003 (2003).
  - [8] W. M. Itano and N. F. Ramsey, *Sci. Am.* **269**, 56 (1993).
  - [9] J. I. Cirac and P. Zoller, *Phys. Rev. Lett.* **74**, 4091 (1995).
  - [10] E. M. Furst and A. P. Gast, *Phys. Rev. Lett.* **82**, 4130 (1999).
  - [11] B. Liu *et al.*, *Phys. Plasmas* **10**, 9 (2003).
  - [12] J. B. Pieper and J. Goree, *Phys. Rev. Lett.* **77**, 3137 (1996).
  - [13] S. Nunomura, D. Samsonov, and J. Goree, *Phys. Rev. Lett.* **84**, 5141 (2000).
  - [14] G. Piacente, F. M. Peeters, and J. J. Betouras, *Phys. Rev. E* **70**, 036406 (2004).
  - [15] B. Liu, K. Avinash, and J. Goree, *Phys. Rev. E* **69**, 036410 (2004).
  - [16] G. A. Hebner, M. E. Riley, D. S. Johnson, Pauline Ho, and R. J. Buss, *Phys. Rev. Lett.* **87**, 235001 (2001).

- [17] G. E. Morfill *et al.*, Phys. Rev. Lett. **83**, 1598 (1999).
- [18] U. Konopka, G. E. Morfill, and L. Ratke, Phys. Rev. Lett. **84**, 891 (2000).
- [19] D. K. C. MacDonald, *Noise and Fluctuations: An Introduction* (Wiley, New York, 1962).
- [20] M. S. Murillo and D. O. Gericke, J. Phys. A **36**, 6273 (2003).
- [21] J. P. Hansen and I. R. McDonald, *Theory of Simple Liquids* (Academic Press, London, 1986).
- [22] M. P. Allen and D. J. Tildesley, *Computer Simulation of Liquids* (Oxford University Press, New York, 1987).
- [23] R. Zwanzig and N. K. Ailawadi, Phys. Rev. **182**, 280 (1969).
- [24] D. Samsonov, J. Goree, H. M. Thomas, and G. E. Morfill, Phys. Rev. E **61**, 5557 (2000).
- [25] R. A. Quinn and J. Goree, Phys. Rev. E **61**, 3033 (2000).
- [26] F. Melandsø, Phys. Plasmas **3**, 3890 (1996).
- [27] S. V. Vladimirov, P. V. Shevchenko, and N. F. Cramer, Phys. Rev. E **56**, R74 (1997).
- [28] A. V. Ivlev and G. E. Morfill, Phys. Rev. E **63**, 016409 (2000).
- [29] A. Siber, Phys. Rev. B **66**, 235414 (2002).